J|A|C|S
ARTICLES
Published on Web 01/25/2007

Radiationless Decay of Red Fluorescent Protein Chromophore Models via Twisted Intramolecular Charge-Transfer States

Seth Olsen* and Sean C. Smith

Contribution from the Centre for Computational Molecular Science, Australian Institute of Bioengineering and Nanotechnology, The University of Queensland, Brisbane, QLD 4072 Australia

Received October 31, 2006; E-mail: s.olsen1@uq.edu.au

Abstract: We use CASSCF and MRPT2 calculations to characterize the bridge photoisomerization pathways of a model red fluorescent protein (RFP) chromophore model. RFPs are homologues of the green fluorescent protein (GFP). The RFP chromophore differs from the GFP chromophore via the addition of an *N*-acylimine substitution to a common *hydroxybenzylidene-imidazolinone* (HBI) motif. We examine the substituent effects on the manifold of twisted intramolecular charge-transfer (TICT) states which mediates radiationless decay via bridge isomerization in fluorescent protein chromophore anions. We find that the substitution destabilizes states associated with isomerization about the imidazolinone-bridge bond and stabilizes states associated with phenoxy-bridge bond isomerization. We discuss the results in the context of chromophore conformation and quantum yield trends in the RFP subfamily, as well as recent studies on synthetic models where the acylimine has been replaced with an olefin.

Introduction

Members of the DsRed-like subfamily of green fluorescent protein (GFP) homologues[1,2] (which we call the red fluorescent proteins, or RFPs) possess a chromophore which contains an *N*-acylimine substituent to a *p-hydroxybenzylidine-imidazolinone* (HBI) motif[3] which is the chromophore functionality in GFPs. The acylimine extends the HBI π electron network and induces a red shift to the absorption and emission relative to GFPs. The range of absorption and emission wavelengths in the RFPs spans from ~550 nm to ~600 nm and from ~575 nm to ~660 nm, respectively.[4] These wavelengths exist on the blue edge of a band with a low extinction coefficient in biological tissue,[5] promoting interest in the development of bright, far-red RFPs for *in vivo* imaging applications.[6] Improved RFPs would also find use as FRET acceptors[7] or in multicolor imaging.[8] Rational development of improved RFPs depends on a solid base of knowledge of the chemical physics of the chromophore functionality. This will be a reference by which to determine how interactions with the protein influence fluorescence color and quantum yield. The fact that several deep-red proteins have been developed from nonfluorescent chromoproteins[9,10] indicates that these interactions may not be separable.

The RFP chromophore, like the GFP chromophore, forms autocatalytically from a tripeptide motif of the form XXG (positions 65−67 in the DsRed sequence).[3] In most naturally occurring RFPs the residue at position 66 is tyrosine, though functional proteins with substitutions in this position have been reported.[11] The acylimine forms after the core HBI motif.[3] In most native RFPs at physiological pH, the chromophore is in an anionic charge state.[3,12] The RFP chromophore resides on the interior of a rigid β-can tertiary structure[13−15] similar to the case for GFP.[16,17] Oligomerization, particularly tetramerization, is common in naturally occurring RFPs, though functional monomeric variants exist.[11] The GFP and RFP chromophore functionalities are displayed in Figure 1. Two resonance forms can be drawn for the GFP chromophore anion. These resonance structures differ by formal bond alternation and by the localization of the formal charge on either the phenoxy (P^-) or imidazolinone (I^-) oxygen. For RFP chromophores a third

(1) Tsien, R. Y. *Annu. Rev. Biochem.* **1998**, *67*, 509.
(2) Verkusha, V. V.; Lukyanov, K. A. *Nat. Biotechnol.* **2004**, *22*, 289.
(3) Gross, L. A.; Baird, G. S.; Hoffman, R. C.; Baldridge, K. K.; Tsien, R. Y. *Proc. Natl. Acad. Sci. U.S.A.* **2000**, *97*, 11990.
(4) Labas, Y. A.; Gurskaya, N. G.; Yanushevich, Y. G.; Fradkov, A. F.; Lukyanov, K. A.; Lukyanov, S. A.; Matz, M. V. *Proc. Natl. Acad. Sci. U.S.A.* **2002**, *99*, 4256.
(5) Weissleder, R.; Ntziachristos, V. *Nature Med.* **2003**, *9*, 123.
(6) Chudakov, D. M.; Lukyanov, S.; Lukyanov, K. A. *Trends Biotechnol.* **2005**, *23*, 605.
(7) Erickson, M. G.; Moon, D. L.; Yue, D. T. *Biophys. J.* **2003**, *85*, 599.
(8) Vonesch, C.; Aguet, F.; Vonesch, J. L.; Unser, M. *IEEE Signal Processing Magazine* **2006**, *23*, 20.
(9) Shkrob, M. A.; Yanushevich, Y. G.; Chudakov, D. M.; Gurskaya, N. G.; Labas, Y. A.; Poponov, S. Y.; Mudrik, N. N.; Lukyanov, S.; Lukyanov, K. A. *Biochem. J.* **2005**, *392*, 649.
(10) Bulina, M. E.; Chudakov, D. M.; Mudrik, N. N.; Lukyanov, K. A. *BMC Biochem.* **2002**, *3*, 7.
(11) Shaner, N. C.; Campbell, R. E.; Steinbach, P. A.; Giepmans, B. N. G.; Palmer, A. E.; Tsien, R. Y. *Nat. Biotechnol.* **2004**, *22*, 1567.
(12) Olsen, S.; Prescott, M.; Wilmann, P.; Battad, J.; Rossjohn, J.; Smith, S. C. *Chem. Phys. Lett.* **2006**, *420*, 507.
(13) Wilmann, P. G.; Battad, J.; Beddoe, T.; Olsen, S.; Smith, S. C.; Dove, S.; Devenish, R. J.; Rossjohn, J.; Prescott, M. *Photochem. Photobiol.* **2006**, *82*, 359.
(14) Pletneva, N.; Pletnev, S.; Tikhonova, T.; Popov, V.; Martynov, V.; Pletnev, V. *Acta. Crystallogr., Sect. D* **2006**, *62*, 527.
(15) Wilmann, P. G.; Petersen, J.; Pettikiriarachchi, A.; Buckle, A. M.; Smith, S. C.; Olsen, S.; Perugini, M. A.; Devenish, R. J.; Prescott, M.; Rossjohn, J. *J. Mol. Biol.* **2005**, *349*, 223.
(16) Yang, F.; Moss, L. G.; George, N.; Phillips, J. *Nat. Biotechnol.* **1996**, *14*, 1246.
(17) Brejc, K.; Sixma, T. K.; Kitts, P. A.; Kain, S. R.; Tsien, R. Y.; Ormö, M. *Proc. Natl. Acad. Sci. U.S.A.* **1996**, *94*, 2306.

10.1021/ja066430s CCC: $37.00

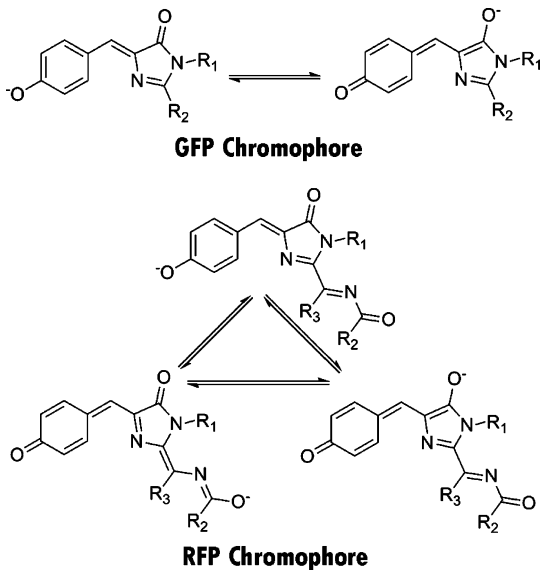

Figure 1. Resonance forms of the GFP chromophore anion (top) and the RFP chromophore anion (bottom). Structures of the GFP chromophore localize the excess charge on the phenoxy oxygen (P^-) or the imidazolinone oxygen (I^-). For the RFP chromophore a third structure which localizes the charge on the acylimine oxygen (A^-) is also possible.

resonance structure may be drawn which localizes the excess charge on the acylimine (A^-).

The fluorescence quantum yield of the RFPs appears correlated to the structure of the chromophore in different proteins. Specifically, nonfluorescent RFPs possess a *trans* chromophore that is nonplanar across the exocyclic bridge. DsRed ($\Phi_{QY} = 0.7$) possesses a *cis* coplanar chromophore.[18,19] The protein EqFP611 ($\Phi_{QY} = 0.45$) carries a chromophore in a *trans* coplanar conformation.[20] Rtms5 and its fluorescent H146S mutant[21] possess a *trans* noncoplanar chromophore with a twist about the phenoxy-bridge bond.[22] The HcRed[23] crystal structure[15] reveals a mixture of *cis* coplanar and *trans* noncoplanar chromophores, corresponding to overlapping peaks in the excitation spectrum. The strongly fluorescent state has been assigned to the *cis* coplanar form. Similar patterns also occur in GFP homologues which do not belong to the RFP subfamily, for example, amFP486,[24] asCP595[25] and the kindling fluorescent protein(KFP).[26]

The correlation between chromophore conformation and quantum yield is usually explained by invocation of nonradiative decay via photoisomerization of the bridge. These hypotheses are based on the considerable body of computational[27,28] and experimental[19] data indicating that bridge photoisomerization leads to internal conversion in GFP chromophores. This mechanism has been invoked as rationalization for the fast internal conversion observed in GFP chromophore models,[29,30] denatured fluorescent GFPs,[31] and nonfluorescent GFP mutants.[32] The relevance of pathways that have been identified for GFP chromophore models has never been demonstrated for RFP chromophores. Their relevance should not be assumed, as it is possible to synthesize fluorescent derivatives of the HBI motif by addition of appropriate substituents.[33] The goal of this work is to clarify the effects of the acylimine substitution on the photoisomerization pathways that have been identified for GFP chromophore models containing the HBI core motif.

There are two low-lying bridge photoisomerization pathways which have been identified for GFP chromophore models. One path corresponds to isomerization of the imidazolinone-bridge bond ("path **I**"), and the other, via torsion of the phenoxy-bridge bond ("path **P**"). Calculations on the GFP chromophore models the HBI[34−38] anion and *4-hydroxybenzylidene-1,2-dimethylimidazolin-5-one* (HBDI)[39] anion indicate that progress along either pathway leads to twisted geometries which form intermediates on the S_1 surface. These intermediates represent quasistable forms of twisted intramolecular charge-transfer (TICT) states which localize the excess electron on one or the other ring. These stable S_1 intermediates are energetically and conformationally close to S_0/S_1 conical intersection[40] seams which arise due to interaction of TICT states of opposing polarity. Access to these seams allows efficient radiationless decay to the ground electronic state.[38] Due to the unstable nature of *N*-acylimines, no chemically accurate synthetic models of the RFP chromophore have been synthesized. An olefin-substituted model with an isoelectronic π system (*4-hydroxybenzylidene-1-methyl-2-penta-1,4-dien-1-yl-imidazolin-5-one*, HBMPDI) was reported to exhibit weak fluorescence in aqueous solution.[41] Olefins are less electron-withdrawing than acylimines, however, so the relevance of this observation is unclear.

This work describes an *ab initio* quantum chemical investigation of the ground and excited-state surface of a chemically accurate (i.e., acylimine-containing) model of the RFP chromophore motif. We reference our results to previous results that have been established for GFP chromophore models.[34−36,38,39] We find that the acylimine substituent considerably alters the

(18) Tubbs, J. L.; Tainer, J. A.; Getzoff, E. D. *Biochemistry* **2005**, *44*, 9833.
(19) Yarbrough, D.; Wachter, R. M.; Kallio, K.; Matz, M. V.; Remington, S. J. *Proc. Natl. Acad. Sci. U.S.A.* **2001**, *98*, 462.
(20) Petersen, J.; Wilmann, P. G.; Beddoe, T.; Oakley, A. J.; Devenish, R. J.; Prescott, M.; Rossjohn, J. *J. Biol. Chem.* **2003**, *278*, 44626.
(21) Dove, S. G.; Takabayashi, M.; Hoegh-Guldberg, O. *Biol. Bull.* **1995**, *189*, 288.
(22) Prescott, M.; Ling, M.; Beddoe, T.; Oakley, A. J.; Dove, S.; Hoegh-Guldberg, O.; Devenish, R. J.; Rossjohn, J. *Structure* **2003**, *11*, 275.
(23) Fradkov, A. F.; Verkhusha, V. V.; Staroverov, D. B.; Bulina, M. E.; Yanushevich, Y. G.; Martynov, V. I.; Lukyanov, S.; Lukyanov, K. A. *Biochem. J.* **2002**, *368*, 17.
(24) Henderson, J. N.; Remington, S. J. *Proc. Natl. Acad. Sci. U.S.A.* **2005**, *102*, 12712.
(25) Wilmann, P. G.; Petersen, J.; Devenish, R. J.; Prescott, M.; Rossjohn, J. *J. Biol. Chem.* **2005**, *280*, 2401.
(26) Quillin, M. L.; Anstrom, D. M.; Shu, X.; O'Leary, S.; Kallio, K.; Chudakov, D. M.; Remington, S. J. *Biochemistry* **2005**, *44*, 5774.
(27) Weber, W.; Helms, V.; McCammon, J. A.; Langhoff, P. W. *Proc. Natl. Acad. Sci. U.S.A.* **1999**, *96*, 6177.
(28) Voituyk, A. A.; Michel-Beyerle, M.; Rösch, N. *Chem. Phys. Lett.* **1998**, *296*, 269.
(29) Niwa, H.; Inouye, S.; Hirano, T.; Matsuno, T.; Kojima, S.; Kubota, M.; Ohashi, M.; Tsuji, F. I. *Proc. Natl. Acad. Sci. U.S.A.* **1996**, *93*, 13617.
(30) Litvinenko, K. L.; Webber, N. M.; Meech, S. R. *J. Phys. Chem.* **2003**, *107A*, 2616.
(31) Ward, W. W.; Bokman, S. H. *Biochemistry* **1982**, *21*, 4535.
(32) Kummer, A.; Kompa, C.; Lossau, H.; Pöllinger-Dammer, F.; Michel-Beyerle, M.; Silva, C. M.; Bylina, E. J.; Coleman, W. J.; Yang, M. M.; Youvan, D. C. *Chem. Phys.* **1998**, *237*, 183.
(33) Follenius-Wund, A.; Bourotte, M.; Schmitt, M.; Iyice, F.; Lami, H.; Bourguignon, J.-J.; Haiech, J.; Pigault, C. *Biophys. J.* **2003**, *85*, 1839.
(34) Martin, M. E.; Negri, F.; Olivucci, M. *J. Am. Chem. Soc.* **2004**, *126*, 5452.
(35) Toniolo, A.; Olsen, S.; Manohar, L.; Martinez, T. J. *Faraday Discuss.* **2004**, *129*, 149.
(36) Toniolo, A.; Granucci, G.; Martinez, T. J. *J. Phys. Chem.* **2003**, *107A*, 3822.
(37) Olsen, S.; Toniolo, A.; Ko, C.; Manohar, L.; Lamothe, K.; Martinez, T. J. Computation of Reaction Mechanisms and Dynamics in Photobiology. In *Computational Photochemistry*; Olivucci, M., Ed.; Elsevier: Amsterdam, 2005.
(38) Olsen, S. The Electronic Excited States of Green Fluorescent Protein Chromophore Models. Ph.D. Thesis, The University of Illinois at Urbana-Champaign, 2004.
(39) Altoe, P.; Bernardi, F.; Garavelli, M.; Orlandi, G.; Negri, F. *J. Am. Chem. Soc.* **2005**, *127*, 3952.
(40) Yarkony, D. R. *Rev. Mod. Phys.* **1996**, *68*, 985.
(41) He, X.; Bell, A. F.; Tonge, P. J. *Org. Lett.* **2002**, *4*, 1523.

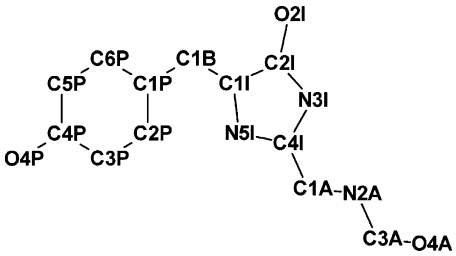

Figure 2. Numbering scheme for the atomic sites of $\mathbf{R_0}$.

energies of states in the charge-transfer manifold which mediates internal conversion via bridge isomerization. These effects manifest themselves in a raising of the S_1 surface in regions associated with photoisomerization of the imidazolinone-bridge bond (path **I**). Conversely, regions associated with photoisomerization of the phenoxy-bridge bond (path **P**) are stabilized, inducing early convergence with an S_0/S_1 conical intersection seam at intermediate values of the bond torsion. An analogue of the intermediate which is found along path **I** in HBI[34−36,38] and HBDI[39] is only marginally accessible on the S_1 surface of our RFP chromophore model. An associated minimal energy conical intersection point lies above the Frank−Condon region on the S_1 surface. There is no phenoxy-twisted intermediate on the S_1 surface of our model RFP chromophore; path **P** leads directly to the intersection seam, which lies at the bottom of the corresponding basin on the S_1 state. We discuss these results in the context of hypotheses which relate nonplanar chromophores to reduced fluorescence in RFPs as well as mechanisms for certain photoconversion processes within the subfamily.[22,42,43] We review implications for the transferability of conclusions drawn from experiments using olefin-substituted synthetic models.[44]

Methods

The results which we report were generated using a model of the RFP chromophore functionality which is truncated to include only the π system of the chromophore. Connections which would be made to the protein backbone or the position 65 side chain (groups R_1, R_2, and R_3 in Figure 1) are terminated by hydrogens. We refer to this model as $\mathbf{R_0}$. We have analyzed the electronic structure of the S_0 and S_1 states of more substantial models and determined that truncation does not change their nature. When referring to our results, we will use a naming scheme for the sites of $\mathbf{R_0}$. This naming scheme is presented in Figure 2.

Our results were generated using state-averaged complete active space self-consistent field theory (SA-CASSCF).[45,46] These results were supplemented (where appropriate) by the use of the internally contracted multireference Rayleigh−Schrödinger second-order perturbation theory (MRPT2).[47] The CASSCF active space contains 12 electrons in 11 orbitals. Ideally, one would like to use an active space which contains the entire valence space or, barring that, the entire space of π orbitals. Both of these goals are unfeasible with the computational resources at our disposal. We have chosen a subset of the π orbitals for our active space. Our choice of orbitals was guided by orbital energies and occupation numbers which were obtained in a preliminary battery of self-consistent field calculations. The resulting orbitals concentrate their amplitude on the CC and CN bonds of the model, which is broadly consistent with resonance Raman analyses of model RFP and GFP chromophores.[48] In general, the results of CASSCF calculations depend on the active space. There may be multiple local solutions to the CASSCF equations even for moderate to large active spaces,[49] and problems may be compounded by the use of state-averaging.[50] In order to facilitate reproducibility, we include graphical representations of the active space orbitals and occupation numbers for each of the potential surface extrema as Supporting Information. We also provide absolute S_0 and S_1 energies and geometries in Cartesian coordinates. The states which were included in the average were the two lowest-lying singlet states S_0 and S_1. Preliminary calculations with other methods identify S_1 as the optically active excited state. For all the results reported here, a 6-31G* Gaussian basis set was employed.[51−53] Preliminary calculations with basis sets including diffuse functions did not indicate significant valence-Rydberg mixing in the S_1 state. Electronic structure calculations were performed using MOLPRO.[54]

For the most part, we will concentrate on results obtained with a model with the CO bond of the acylimine in a *cis* position relative to the imine lone pair. This has been determined to be the relevant orientation in native RFPs.[18] We have also investigated a model with a *trans* acylimine conformation and have found that the results are qualitatively identical. Where it is more convenient or illustrative, we will quote results obtained with the *trans* acylimine model. Optimized geometries, SA-CASSCF and MRPT2 energies, and active space orbital descriptions for the *trans*-acylimine conformer are included as Supporting Information.

We will investigate the effect of acylimine substitution on the HBI photoisomerization via an examination of coordinate-driving representations of the hypothetical pathways **P** and **I**. Coordinate-driving potential surface scans were generated by fixing one (or both) of the two bridge dihedrals (the driven coordinates) of $\mathbf{R_0}$ and minimizing all other degrees of freedom subject to this constraint. The first driven coordinate, ϕ_P, is the dihedral angle defined by sites C2P−C1P−C1B−C1I in our naming convention and represents progress along a hypothetical path **P** leading to photoisomerization of the phenoxy-bridge bond. The second, ϕ_I, is defined by sites C1P−C1B−C1I−N5I and represents progress along a hypothetical path **I** leading to photoisomerization of the imidazolinone-bridge bond. As we will show, path **I** is strongly disfavored compared to path **P**. This results in a tendency to twist the phenoxy-bridge bond in the excited state at small values of the imidazolinone-bridge torsion ϕ_I. In order to generate clearly distinguishable reaction coordinates for each bond, the phenoxy-bridge dihedral ϕ_P was constrained to zero along the coordinate-driven representation of path **I**. The coordinate-driven model of path **I** therefore represents an approximation in a more restrictive limit than for path **P**, for which only the ϕ_p dihedral was constrained. This does not substantially impact our principle results; it is the TICT state itself which is energetically disfavored and not any particular hypothetical reaction path. The use of coordinate driving potential scans to model reaction coordinates can be problematic if the driven coordinate is not a good representation of the true reaction coordinate. In such cases the relevant barriers can be missed.[55] This problem may manifest itself as a sudden change in degrees of freedom belonging to the set which is complementary to the driven coordinate. Barriers along the coordinate-driving pathways

(42) Loos, D. C.; Habuchi, S.; Flors, C.; Hotta, J.-i.; Wiedenmann, J.; Nienhaus, G. U.; Hofkens, J. *J. Am. Chem. Soc.* **2006**, *128*, 6270.
(43) Habuchi, S.; Cotlet, M.; Gensch, T.; Bednarz, T.; Haber-Pohlmeier, S.; Rozenski, J.; Dirix, G.; Michiels, J.; Vanderleyden, J.; Heberle, J.; DeSchryver, F. C.; Hofkens, J. *J. Am. Chem. Soc.* **2005**, *127*, 8977.
(44) Boyé, S.; Krogh, H.; Nielsen, I. B.; Nielsen, S. B.; Pedersen, S. U.; Pedersen, U. V.; Andersen, L. H.; Bell, A. F.; He, X.; Tonge, P. J. *Phys. Rev. Lett.* **2003**, *90*, 118103.
(45) Docken, K. K.; Hinze, J. *J. Chem. Phys.* **1972**, *57*, 4928.
(46) Roos, B. O.; Taylor, P. R.; Siegbahn, P. E. M. *Chem. Phys.* **1980**, *48*, 157.
(47) Celani, P.; Werner, H.-J. *J. Chem. Phys.* **2000**, *112*, 5546.
(48) Boyé, S.; Nielsen, S. B.; Krogh, H.; Nielsen, I. B.; Pedersen, U. V.; Bell, A. F.; Xiang, He; Tonge, P. J.; Andersen, L. H. *Phys. Chem. Chem. Phys.* **2003**, *5*, 3021.
(49) Guihery, N.; Malrieu, J.-P.; Maynau, D.; Handrick, K. *Int. J. Quant. Chem.* **1997**, *61*, 45.
(50) Zaitsevskii, A.; Malrieu, J.-P. *Chem. Phys. Lett.* **1994**, *228*, 458.
(51) Hehre, W. J.; Ditchfield, R.; Pople, J. A. *J. Chem. Phys.* **1972**, *56*, 2257.
(52) Frisch, M. J.; Pople, J. A.; Binkley, J. S. *J. Chem. Phys.* **1984**, *80*, 3265.
(53) Krishnan, R.; Binkley, J. S.; Pople, J. A. *J. Chem. Phys.* **1980**, *72*, 650.
(54) Werner, H.-J., et al. *MOLPRO*, version 2002.6, a package of ab initio programs.

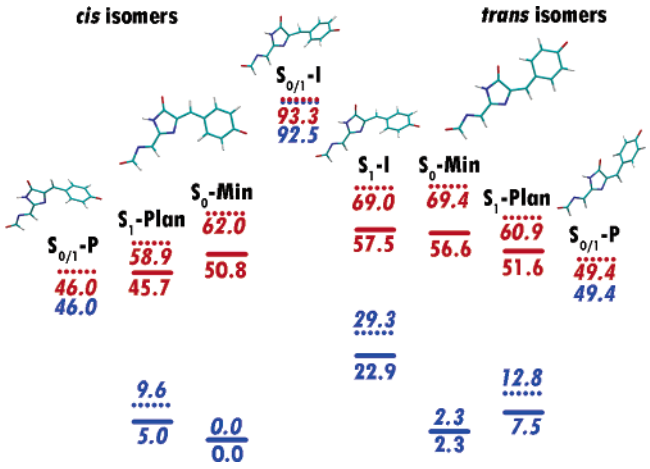

Figure 3. Energies of potential surface extrema for model $\mathbf{R_0}$. SA-CASSCF energies are graphically depicted as dotted lines and enumerated as italicized text. MRPT2 energies are graphically depicted by solid lines and plain text. Red lines and text refer to S_1 energies, and blue lines and text refer to S_0 energies. Pictures of the structures are displayed at the top of the figure. Pictures of planar conformers are consolidated for economy of space. All energies are in kcal/mol relative to the *cis* S_0 minimum. Shorthand nomenclature for the geometries is indicated in black text.

can be considered as upper bounds to true activation energies. Our primary goal was to investigate the effects of acylimine substitution on previously established pathways for HBI-containing models. Coordinate-driving representations of the pathways should be adequate for this purpose.

The implementation of multireference perturbation theory which we have used here is not a true "multistate" perturbation theory (i.e., of the "diagonalize−perturb−diagonalize" variety).[56,57] As such, it is not expected to perform well in the vicinity of intersections between states which span the model space.[58] In order to avoid confusion, we do not quote MRPT2 energies at geometries where the energies of the zeroth order states are degenerate (i.e., at conical intersections). We do not expect any of the methods we use here to yield energy differences to an accuracy of less than 1 kcal/mol.[59] Energy differences below this threshold should not be considered conclusive.

Results

Extrema of the S_0 and S_1 Surfaces: Energetics and Geometries. We have optimized five minima and three minimal energy conical intersection (MECI) structures on the S_0 and S_1 surfaces of $\mathbf{R_0}$. These include, for each of the *cis* and *trans* conformers, a minimum on S_0 (S_0-Min), a planar minimum on S_1 (S_1-Plan), and a S_0/S_1 MECI which is twisted about the phenoxy-bridge (C1B−C1P) bond ($S_{0/1}$-P). We have also located an S_1 minimum (S_1-I) and a minimal energy conical intersection ($S_{0/1}$-I) which feature substantial twist about the imidazolinone-bridge bond. The former represents an intermediate between *cis* and *trans* forms on S_1. S_1 and S_0 energies at the optimized geometries are graphically summarized in Figure 3. Figure 4 displays the optimized geometries, with heavy atom bond lengths listed next to the bonds they represent.

The S_0-Min geometries of $\mathbf{R_0}$ reflect the threefold resonance of the RFP chromophore (Figure 1), featuring a short phenoxy-bridge bond and a quinone-like character to the phenoxy bond alternation. This formal bond alternation suggests contributions

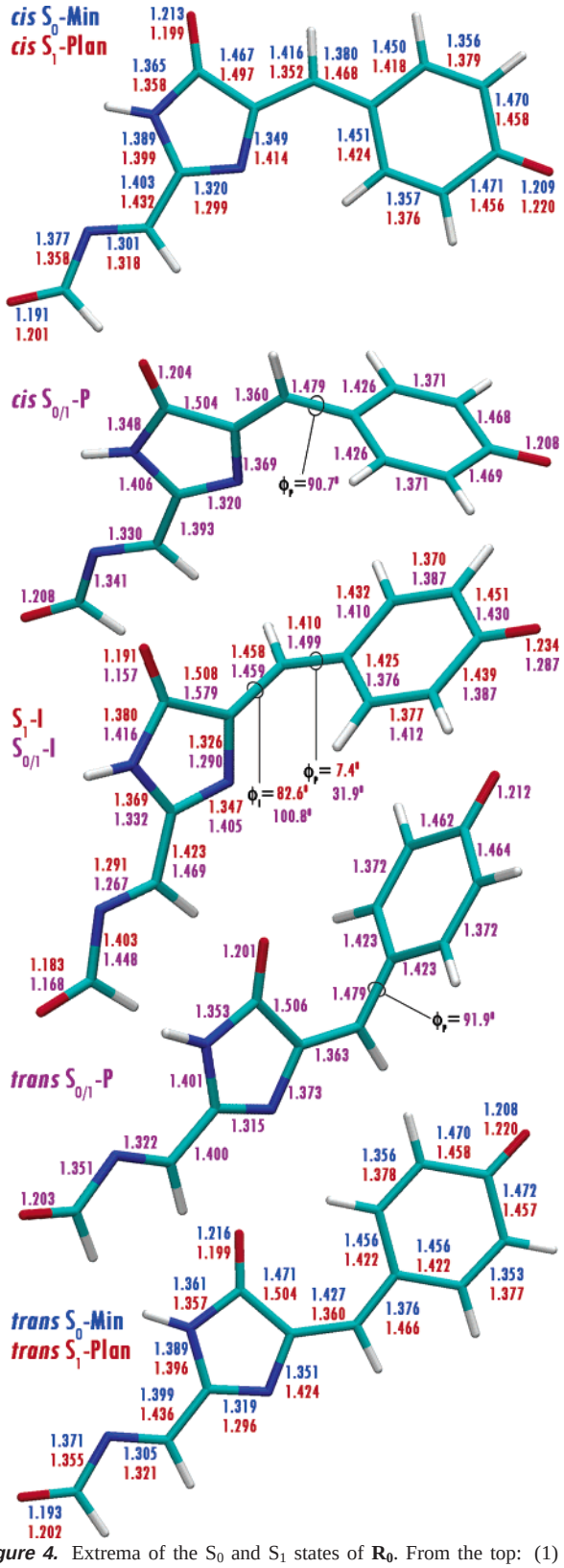

Figure 4. Extrema of the S_0 and S_1 states of $\mathbf{R_0}$. From the top: (1) *cis* planar S_0 (*cis*-S_0-Min) and S_1 (*cis*-S_1-Plan) minima; (2) *cis* phenoxy-twisted S_0/S_1 MECI ($S_{0/1}$-P); (3) imidazolinone-twisted S_1 minimum (S_1-I) and S_0/S_1 MECI ($S_{0/1}$-I); (4) *trans* phenoxy-twisted S_0/S_1 MECI (*trans*-$S_{0/1}$-P); (5) *trans* planar S_0 (*trans*-S_0-Min) and S_1 (*trans*-S_1-Plan) minima. Heavy atom bond lengths are displayed next to their respective bonds in blue for S_0 extrema, red for S_1 extrema, and purple for S_0/S_1 intersection structures.

(55) Bondar, N.; Elstner, M.; Fischer, S.; Smith, J. C.; Suhai, S. *Phase Transitions* **2004**, *77*, 47.
(56) Finley, J.; Malmqvist, P.-A.; Roos, B. O.; Serrano-Andres, L. *Chem. Phys. Lett.* **1998**, *288*, 299.
(57) Shavitt, I. *Int. J. Mol. Sci.* **2002**, *3*, 639.
(58) Serrano-Andres, L.; Merchan, M.; Lindh, R. *J. Chem. Phys.* **2005**, *122*, 104107.
(59) Andersson, K.; Malmqvist, P.-A.; Roos, B. O. *J. Chem. Phys.* **1992**, *96*, 1218.

by the resonance structures I^- and A^-. The contribution of A^--like structures is also indicated by the vicinal CC bond on the imidazolinone and by altered bond alternation on the imine relative to HBI.[34] Relaxation on the S_1 state yields the S_1-Plan geometries, where the bridge alternation is inverted and the quinone-like character of the phenoxy is reduced. The imidazolinone bond lengths change in a qualitatively similar fashion for both *cis* and *trans* conformers of **R_0**. The change in of the N5I−C4I and C1I−N5I bonds after relaxation on the S_1 state is opposite to that observed for the HBI anion. On the acylimine, the C4I−C1A, C1A−N2A, and C3A−O4A bonds lengthen on the excited state, while the N2A−C3A bond contracts. At the S_0-Min structure, the C4P−O4P bond is shorter than the C2I−O2I bond, as in the case for HBI. The CO bond alternation inverts upon relaxation in the S_1 surface, as is also the case for the HBI and HBDI anion.

The MRPT2 excitation energies at the S_0-Min geometries are 54.2 kcal/mol (2.35 eV, 527 nm) and 50.7 kcal/mol (2.20 eV, 563 nm) for the *trans* and *cis* conformers, respectively. At the S_1-Plan geometries, these excitations are shifted downward to 44.0 kcal/mol (1.91 eV, 648 nm) and 40.8 kcal/mol (1.77 eV, 702 nm). The excitation energies at S_0-Min for the different conformers straddle the blue edge of the absorption range of known RFPs and the gas phase absorption maximum of the synthetic model HBMPDI.[44] The excitation energies at S_1-Plan straddle the red edge of the emission range of known RFPs.[4] The Stokes shifts are slightly higher than those observed for HBMPDI in solution and are on par with the largest shifts seen in RFPs with anionic chromophores.[60,61]

The phenoxy twisted MECIs ($S_{0/1}$-P) are characterized by a nearly 90° twist of the ϕ_P dihedral angle and elongated phenoxy-bridge bonds. The acylimine C3A−O4A bond is longer than that at the S_1-Plan geometries, but the phenoxy C4P−O4P and imidazolinone C2I−O2I bonds are shorter. The bond length alternation on the phenoxy shows intermediate quinone character compared to S_0-Min and S_1-Plan. There is no significant pyramidalization of the carbons involved in the bridge bonds, and apart from the single twisted bond, the molecule is planar. The bond lengths are close to C_S symmetry.

The (SA-CASSCF) energetics of the $S_{0/1}$-P structures show them to be energetically accessible on S_1 from either the S_0-Min or S_1-Plan geometries. The magnitude of the descent on the S_1 state is smaller than the magnitude of the ascent on S_0 for both conformers. The S_1 energy difference between the S_1-Plan and $S_{0/1}$-P geometries is larger for the *trans* form (−11.5 kcal/mol) than for the *cis* (−7.9 kcal/mol).

The S_1-I geometries show a slight "hula-twist" character,[62] with a ϕ_I angle of 82.6° and a ϕ_P angle of −7.4°, and a pyramidalization of the bridge carbon. The phenoxy ring shows reduced quinone-like character. The CO bonds on the acylimine, imidazolinone, and phenoxy moieties grow progressively longer in that order. The bond alternation in the acylimine is stronger than in the planar or phenoxy-twisted structures.

The SA-CASSCF energy of the S_1-I geometry is 0.4 kcal/mol less than the S_1 energy of the *trans* S_0-Min geometry. This energy ordering inverts at the MRPT2 level, but the difference remains less than 1 kcal/mol. This energy difference is below the expected accuracy of the method we have used to evaluate the energetics.[34] We cannot unambiguously determine if the S_1-I geometry is energetically accessible from *trans* S_0-Min in a dissipation-free environment. In the presence of dissipative forces, S_1-I is not likely to be accessible. It is not accessible from the *trans* S_1-Plan geometry or from either of the planar *cis* geometries. These results indicate that structures like S_1-I will not play a significant role in nonactivated gas-phase photoprocesses of molecules similar to **R_0**. Such structures may play a part in activated excited-state processes.

The $S_{0/1}$-I MECI shows a more pronounced hula-twist character than the S_1-I structure, with ϕ_I and ϕ_P angles of 100.8° and −31.9°, respectively. The pyramidalization of the bridge carbon is more severe. The C1I−C1B bond is nearly the same as the S_1-I structure, while the C1B−C1P bond is noticeably longer. The phenoxy moiety displays a Kekulé-like bond alternation. The bond lengths on the imidazolinone represent extreme values in comparison with other structures, and the bond alternation on the acylimine is more pronounced.

The (SA-CASSCF) S_0-S_1 energy difference at this geometry is 0.8 kcal/mol, which is consistent with an intersection within our 1 kcal/mol accuracy limit. The $S_{0/1}$-I geometry is 24.3 kcal/mol higher than the S_1-I geometry on the S_1 surface, making it inaccessible from all other geometries we have optimized. We do not expect that it will play a significant role in the nonactivated gas-phase photochemistry of molecules similar to **R_0**.

Electron Density Distributions at the Minima. Figure 5 describes the S_0 and S_1 electron density distribution at the minima which we have optimized via Mulliken charge analysis and S_1-S_0 charge difference density isosurfaces. At the S_0-Min structures, we observe a net gain in electron density in the phenoxy π system associated with excitation to the S_1 state. A depletion of electron density from the C1B−C1P bond is also apparent, as is a slight increase in density on the C1B site and in the C1B−C2I bonding region. The imidazolinone loses net π electron density in the S_1 state. N3I and N5I show a slight gain in electron density, but the invariance of the N5I Mulliken charges suggests that the increase in π density may be countered by a decrease in the σ (and nonbonding) density. The net electron migration to the acylimine upon excitation is small. As the active space used to generate these results contained only orbitals with approximate π symmetry, gain or loss of density from the σ or nonbonding systems must reflect deviations from the strict π character of the orbitals. In treatments that include non-π correlation this effect may be more pronounced.

At the S_1-Plan geometries, the amount of electron density gained by the acylimine upon excitation is increased, and the density on the phenoxy is reduced. The gain on the phenoxy oxygen is much less than that at the S_0-Min geometries. The electron distribution on the imidazolinone is broadly similar to that for S_0-Min.

At the S_1-I geometry, excitation induces a gain in π electron density on the phenoxy and bridge moieties and a loss of density on the imidazolinone and acylimine moieties. An analysis of the Mulliken charge densities reveals that in the S_0 state there is approximately an entire electronic charge localized on the imidazolinone and acylimine moieties. This localization is reversed on the S_1 state. This is consistent with the assignment

(60) Wang, L.; Jackson, W. C.; Steinbach, P. A.; Tsien, R. Y. *Proc. Natl. Acad. Sci. U.S.A.* **2004**, *101*, 16745.
(61) Kogure, T.; Karasawa, S.; Araki, T.; Saito, K.; Kinjo, M.; Miyawaki, A. *Nat. Biotechnol.* **2006**, *24*, 577.
(62) Baffour-Awuah, N. Y. A.; Zimmer, M. *Chem. Phys.* **2004**, *303*, 7.

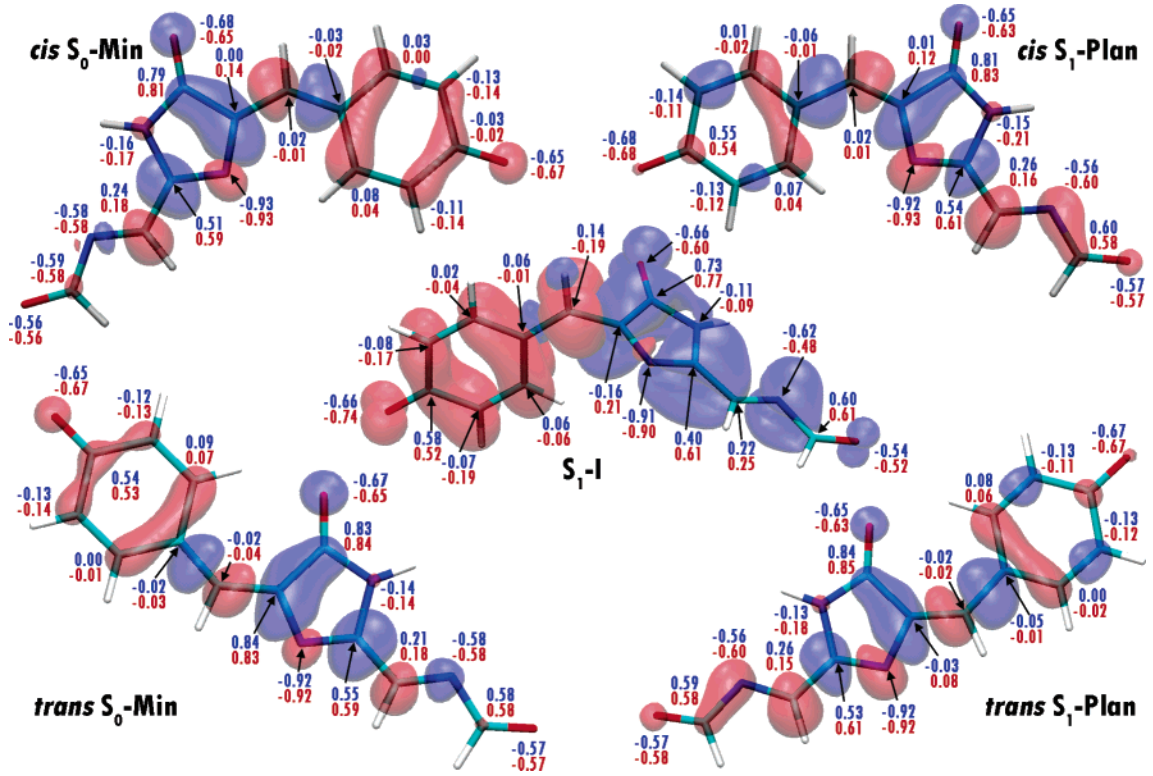

Figure 5. Electron density analyses at the potential surface minima of $\mathbf{R_0}$. Mulliken charges (hydrogens summed to heavy atoms) for the S_0 (blue) and S_1 (red) states are listed next to the atomic sites. S_1-S_0 charge difference isodensity surfaces (isovalue = 0.001) are also displayed with negative isosurfaces in blue and positive isosurfaces in red. Geometries are the *cis* S_0 minimum (*cis*-S_0-Min; top left); *cis* planar S_1 minimum (*cis*-S_1-Plan; top right); *trans* S_0 minimum (*trans*-S_0-Min; bottom left); *trans* planar S_1 minimum (*trans*-S_1-Plan; bottom right); and the imidazolinone-twisted S_1 minimum (S_1-I; center).

of S_1-I as a stable conformation of a diabatic TICT state which dominates the S_1 adiabatic state in this region. This TICT state, which concentrates the electron density on the phenoxy, is the mirror of a TICT state with an opposite charge localization which dominates S_0. No local minimum on the S_0 state could be found with a similar twist.

Electron Density Distributions Near the Intersections. The indeterminacy of the wavefunction at a conical intersection seam and the accompanying distortions at nearby regions make Mulliken or isodensity analysis unreliable. However, given the apparent change in electron localization in the S_0 and S_1 states at the S_1-I geometry, it is relevant to ask whether charge localization is observed at geometries with a twisted phenoxy-bridge bond. An analysis of points in the branching plane[40] of the $S_{0/1}$-P intersections indicates that this is the case and that these intersections join diabatic TICT states with different charge localization characters. A typical situation is illustrated in Figure 6. The figure contains a plot of the S_0 and S_1 energies over an area of the branching plane of the intersection for a *trans* conformer of $\mathbf{R_0}$. The branching plane is spanned by coordinates representing bond alternation ($\bar{g}$) and phenoxy-bridge torsion ($\bar{h}$). There is a pronounced slant in the S_0 state across the branching plane in the direction of the bond alternation, implying photostability with respect to changes in the bond orders.[63] The S_1 energy rises in all directions away from the intersection, consistent with its nature as a local minimum of the S_1 potential surface. As one traverses the intersection seam along the bond alternation coordinate the localization of electronic charge switches from one side of the bond to the other. The sense of localization is opposite in the S_0 and S_1 states. Traversing the plane along the bond torsion coordinate does not change the charge localization. The charge is equally distributed in a band which passes through the intersection along the bond torsion coordinate. This is consistent with an identification of bond torsion as the coordinate which couples the S_0 and S_1 states. The bond alternation coordinate can then be identified with the S_1-S_0 tuning coordinate.

We will not describe the situation near the $S_{0/1}$-I intersection in detail because our results indicate that it would not play a substantial role in the gas-phase photochemistry of this system. However, these intersections are also of charge-transfer character, and the sense of charge localization changes qualitatively across the imidazolinone-bridge bond in a similar fashion. These results are broadly consistent with descriptions of the electronic structure near charge-transfer conical intersections that have been previously reported for the HBI anion.[34−36]

Coordinate-Driving Surface Scans and Potential Surface Slices. In order to provide a more detailed comparison between the $\mathbf{R_0}$ and HBI pathways and between the *cis* and *trans* conformers of $\mathbf{R_0}$, we have generated coordinate-driving potential surface scans using the ϕ_I and ϕ_P dihedral coordinates. The surface scans along the ϕ_P coordinate for *cis* and *trans* conformers are displayed in Figure 7, along with the difference of Mulliken charges summed on either side of the twisting bond. Results from a similar scan along the ϕ_I coordinate are displayed in Figure 8.

The coordinate driven paths **P** for the *cis* and *trans* conformers of model $\mathbf{R_0}$ are consistent with barrierless pathways on S_1 leading from the optically bright Frank−Condon region to TICT states which localize the excess electronic charge on the

(63) Atchity, G. J.; Xantheas, S. S.; Ruedenberg, K. *J. Chem. Phys.* **1991**, *95*, 1862.

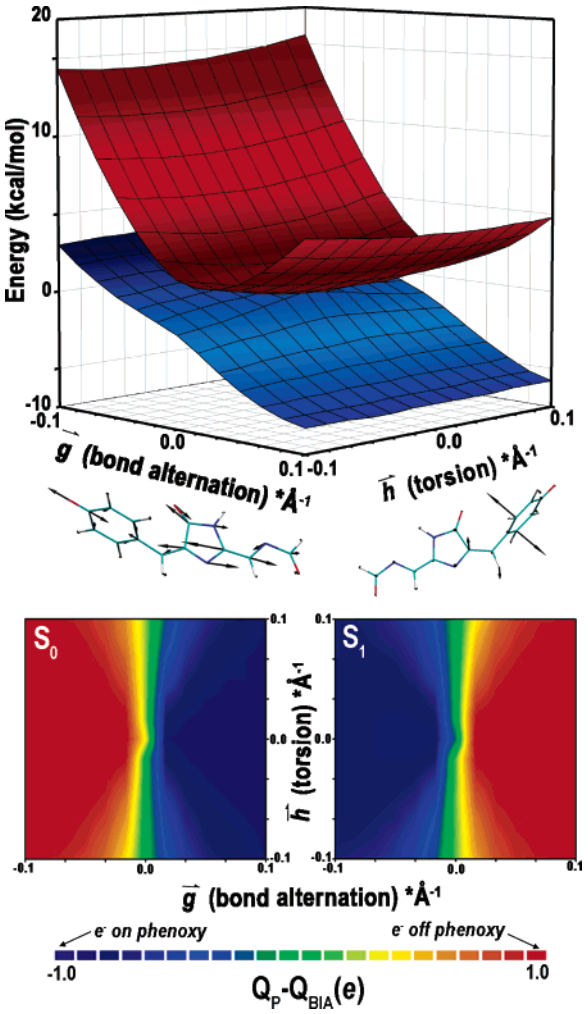

Figure 6. Top: S_0 (blue) and S_1 (red) energies over the branching plane of the phenoxy-twisted MECI of a *trans* conformer of $\mathbf{R_0}$. Graphical descriptions of the branching plane coordinates *g* and *h* are depicted under the respective axes. Bottom: Mulliken charge differences summed on the phenoxy (Q_P) and bridge/imidazolinone/acylimine (Q_{BIA}) sides of the phenoxy-bridge bond in the S_0 (left) and S_1 (right) states over the branching plane. Mulliken charge differences are color-coded: negative charge values (electron localization on the phenoxy) are blue, and positive charge differences (localization off the phenoxy) are red.

imidazolinone side of the bridge. The energies for the *trans* conformer show a rise in S_1 energy (relative to $\phi_P = 0°$) of 0.06 kcal/mol at $\phi_P = 15°$ at the MRPT2 level. At the SA-CASSCF level, there is a rise in S_1 energy which peaks at 0.14 kcal/mol ($\phi_P = 30°$). For the *cis* conformer, there is a rise in S_1 energy that peaks at 0.56 kcal/mol ($\phi_p = 45°$) at the MRPT2 level and 0.44 kcal/mol at the SA-CASSCF level ($\phi_p = 30°$). All of these energy differences are beneath the expected accuracy of the method.[34]

We observe a convergence between our coordinate driven path **P** and an S_0/S_1 conical intersection seam for both conformers. This convergence occurs at ϕ_P values of 67.5° for the *trans* conformer and 87.5° for the *cis* conformer. The seam arises from a crossing between TICT states which localize the charge on the imidazolinone and phenoxy sides of the bridge. The localization of electronic charge on the imidazolinone and acylimine moieties in the S_1 state occurs as the ϕ_p dihedral angle increases past 45°. For the *cis* conformer, the charge difference $Q_P - Q_{AIB}$ is 0.26 *e* on S_0 and 0.65 *e* on S_1 at $\phi_P = 0°$. At $\phi_P = 75°$ the difference on S_0 decreases to -0.64 *e*, representing increased electron localization on the phenoxy moiety, and 1.01 *e* on S_1, representing localization on the imidazolinone and acylimine. A similar trend can be observed in the *trans* conformer, though less data are available due to the earlier convergence with the intersection seam.

The S_1 energy along the coordinate-driven path **I** suggests the presence of a barrier to the imidazolinone-bridge bond torsion. From $\phi_I = 0°$ the S_1 energy shows a consistent rise in S_1 energy which peaks at 12.83 kcal/mol ($\phi_I = 105°$) at the MRPT2 level. The S_1 energy at $\phi_I = 180°$ is 7.00 kcal/mol higher than that at $\phi_I = 0°$ at this level of theory. The rise in energy coincides with the appearance of charge-localized character in the S_1 and S_0 states. In this case, excess charge localizes on the imidazolinone-acylimine side in the S_0 state and on the phenoxy-bridge side in the S_1 state. The charge difference $Q_{PB} - Q_{IA}$ in the S_0 state is 0.28 *e* at $\phi_I = 0°$ and $\phi_I = 180°$ but is equal to 1.11 *e* at $\phi_I = 105°$, representing localization of charge density on the acylimine-imidazolinone side. In the S_1 state the difference is 0.30 *e* at $\phi_I = 0°$ and 0.29 at $\phi_I = 180°$ but decreases to -0.77 *e* at $\phi_I = 90°$, representing concentration of electron density on the phenoxy-bridge side. The contribution of the phenoxy-localized electronic charge in the S_1 state raises the energy of S_1 along the path, inducing the barrier. Our coordinate-driving path **I** model is an approximation corresponding to the limit of zero torsion in the phenoxy-bridge dihedral ϕ_P, and so our estimation of the barrier height is not a rigorous proof that barrierless paths corresponding to imidazolinone-bond isomerization do not exist. However, our data are consistent with a raising of the TICT states which are associated with imidazolinone-bridge bond torsion on the S_1 state.

In order to obtain a better picture of the electronic structure and energetic topology of the surfaces associated with phenoxy-bridge bond isomerization, we generated the two-dimensional potential surface slices and Mulliken charge plots which are displayed in Figure 9. These surface slices were constructed via a bilinear interpolation between either the S_0-Min structure (left) or the S_1-Plan structure (right) and the $S_{0/1}$-P geometry of a *trans* conformer of model $\mathbf{R_0}$. The two surface plots at the top of the figure represent (SA-CASSCF) S_0 and S_1 energies over the slice. The pairs of shaded contour surfaces beneath the energy plots display the difference of Mulliken charges summed on either side of the C1P−C1B bond ($Q_p - Q_{BIA}$) in the S_0 and S_1 states, in similar fashion to Figure 6.

The interpolation plot between S_0-Min and $S_{0/1}$-P geometries reveals that along the entire edge of the plot ϕ_P has a value equal to that found at $S_{0/1}$-P; the energy splitting between the S_0 and S_1 states never exceeds 2.3 kcal/mol. This is above the range which would indicate coincidence with a conical intersection seam, but it may be interpreted as a suggestion of a nearby intersection. The splitting is consistent with an intersection seam (within 1 kcal/mol) for approximately half of the interpolation over the complementary coordinate set. This splitting is far smaller than the splitting over the branching plane featured in Figure 6 (by more than an order of magnitude). The total variation of the S_1 energy along this edge of the plot is 10.7 kcal/mol, roughly equal to the energy difference between the S_1-Plan and $S_{0/1}$-P geometries. The S_0/S_1 splitting along the

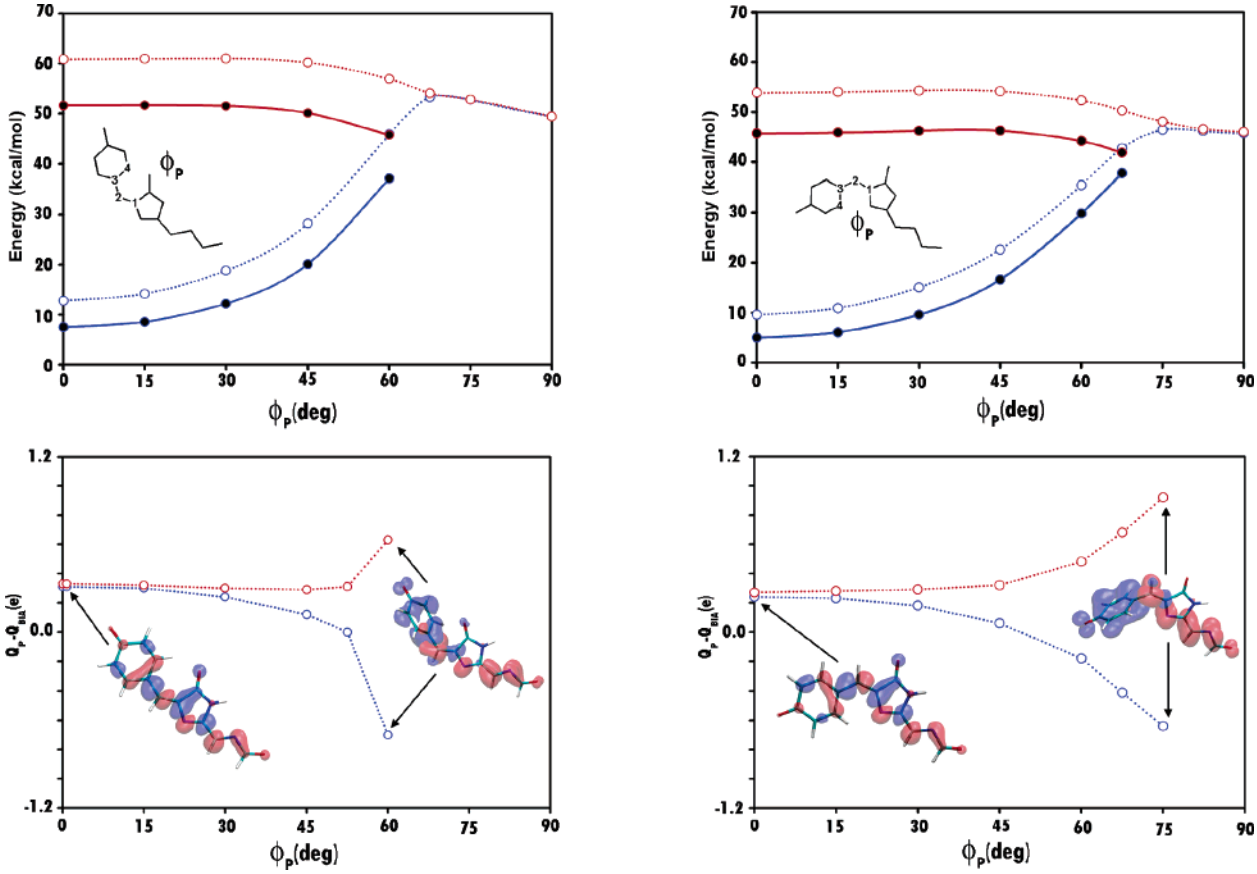

Figure 7. Top: S_0 (blue) and S_1 (red) energies along the phenoxy-twist photoisomerization pathway (Path **P**) of *trans* (left) and *cis* (right) forms of $\mathbf{R_0}$ at the SA-CASSCF (dotted line, ○) and MRPT2 (solid line, ●) levels of theory. Structures along the pathway were generated by optimization on S_1 subject to the constraint of constant ϕ_P dihedral angle. Atoms defining the dihedral are numbered in the figure insets. Bottom: Difference ($Q_P - Q_{BIA}$) of Mulliken charges summed on the phenoxy (Q_P) side and the bridge/imidazolinone/acylimine (Q_{BIA}) of the phenoxy-bridge bond. S_1-S_0 charge density difference isosurfaces (isovalue = ±0.001) are displayed at the $\phi_P = 0°$ point and at the last point prior to convergence with the intersection seam ($\phi_P = 75°$ for the *cis* isomer and $\phi_P = 60°$ for the *trans* conformer). Positive isosurfaces are red, and negative isosurfaces are blue.

analogous edge of the interpolation between S_1-Plan and $S_{0/1}$-P becomes larger, reaching a maximum at 6.7 kcal/mol.

The plots suggest that the intersection seam leading to phenoxy-bridge isomerization may be accessible over a considerable range of the phenoxy-bridge dihedral ϕ_P. Twisting the C1B−C1P bond from planar configurations localizes the charge on the phenoxy in the S_0 state and off the phenoxy in the S_1 state. This is consistent with our results obtained via coordinate driving surface scans, though the onset of localization appears at larger ϕ_P values here. This is an indication that the onset of charge localization depends on more than just the torsion. This is not unexpected. Charge localization corresponds to cleavage of the π bond, which will generally depend on other geometric parameters such as the length of the twisted bond and the pyramidalization of the participating atoms.

Discussion

We have reported the results of *ab initio* multireference quantum chemical characterizations of the S_0 and S_1 electronic states of a truncated model of an RFP ("DsRed-like") chromophore. To our knowledge, these results constitute the first theoretical characterization of bridge isomerization reactions in RFP chromophore models. Significant results arise from the work. The first is that there are favorable bridge isomerization pathways on the S_1 state of a chemically accurate RFP chromophore model. Progress along these pathways is predicted to lead to internal conversion via an S_0/S_1 conical intersection seam. This result is significant because such pathways have already been implicitly or explicitly invoked as rationalization for certain structural and photophysical trends within the RFP subfamily.[22,42,43] Their existence in RFP models has not been demonstrated before now. The fact that fluorescent derivatives of the HBI core motif can be synthesized by the addition of appropriate substituents[33] is evidence that the existence of favorable photoisomerization pathways should not be assumed. In this sense, our results provide an improved foundation for hypotheses which invoke bridge photoisomerization in the RFPs.

The second significant result of our work is the observation that the addition of the *N*-acylimine substituent to the *hydroxybenzylidene-imidazolinone* (HBI) core selectively stabilizes (or destabilizes) certain twisted intramolecular charge-transfer (TICT) states in the manifold which mediates internal conversion via bridge isomerization. Analogous states have been shown to contribute to low-lying photoisomerization pathways of the HBI functionality in isolation[28,34,36] or as part of a synthetic GFP chromophore model HBDI.[39] HBI is the chromophore functionality of GFPs.[4] The bridge isomerization of HBI has been studied by CASSCF and CASPT2 methods;[34,35,38] semiempirical CISD,[28] OM2,[27] and CAS-CI[36] methods using standard parameter sets; and semiempirical CAS-CI using parameters derived from *ab initio* results.[35] The corresponding pathways in HBDI have been investigated using CASSCF and CASPT2 methods

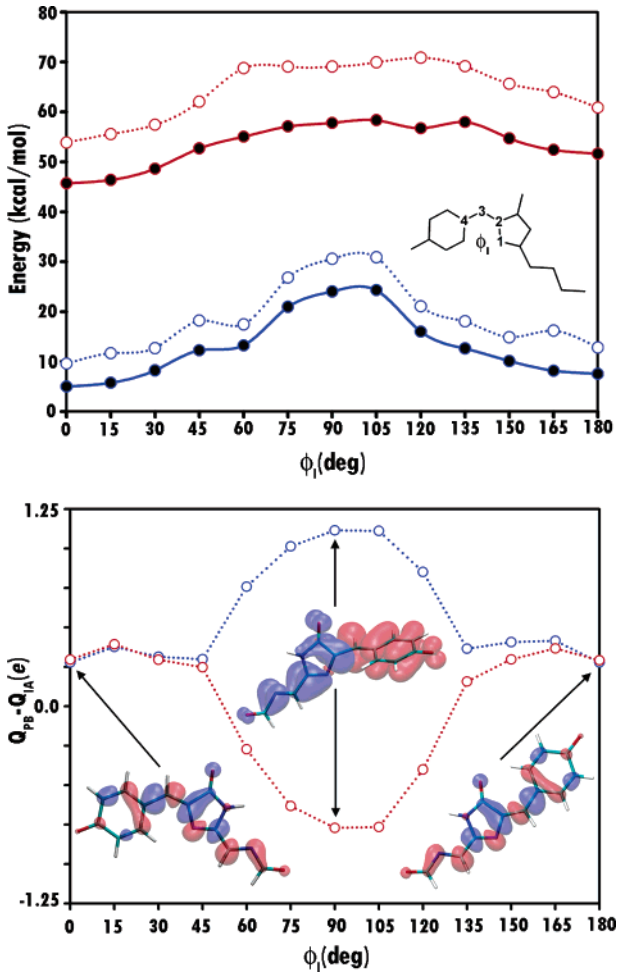

Figure 8. Top: S_0 (blue) and S_1 (red) energies along the imidazolinone-twist photoisomerization pathway (path **I**) of $\mathbf{R_0}$ at the SA-CASSCF (dotted line, ○) and MRPT2 (solid line, ●) levels of theory. Geometries were obtained via optimization on S_1 subject to constraint of constant ϕ_I dihedral angle with $\phi_P = 0$. Atoms defining the dihedral are numbered in the inset. Bottom: The difference between Mulliken charges summed on the phenoxy/bridge (Q_{PB}) and imidazolinone/acylimine (Q_{IA}) sides of the imidazolinone-bridge bond in the S_0 (blue) and S_1 (red) states at the SA-CASSCF level of theory. S_1-S_0 charge difference isodensities (isovalue = ±0.001) at ϕ_I = 0°, 90°, 180° are inset. Positive isosurfaces are red, and negative isosurfaces are blue.

in vacuo and in a polarizable continuum solvent model.[35,37] The results of these studies indicate the presence of two favorable isomerization pathways on S_1, each associated with torsion about a different bridge bond. Progress along these pathways leads to TICT states which localize the excess electronic charge on one side of the twisted bond.

Our results indicate that the acylimine substituent stabilizes TICT states which are associated with photoisomerization of the phenoxy-bridge bond in the S_1 state. TICT states which lead to isomerization of the imidazolinone-bridge bond are concomitantly destabilized. In our truncated model $\mathbf{R_0}$, the conjugation of the imidazolinone and the acylimine delocalizes the electron density across both moieties. The strongly electronegative acylimine lowers the energy of states which localize electron density on the imidazolinone/acylimine side of the bridge and destabilizes states which localize density on the phenoxy side. This has the effect of raising the energy of the S_1 state in regions associated with imidazolinone-bridge bond torsion and lowering it in regions associated with phenoxy-bridge bond torsion. Opposite effects occur for the S_0 state along these pathways, as the sense of charge localization is reversed. The combination of these effects leads to the induction of a seam of conical intersection which intersects a coordinate-driven path **P** at intermediate values of the phenoxy-bridge bond torsion. Analogous conical intersections associated with imidazolinone-bridge bond torsion lie above the Frank−Condon region on the S_1 surface. They are not expected to be accessible without excess energy input.

The results we report here were generated with a highly truncated model of the RFP chromophore functionality considered in isolation from any environment. The most reasonable choice of experimental data for comparison would be gas-phase data obtained with a chemically similar model. Unfortunately *N*-acylimines are unstable species prone to nucleophilic attack, and no acylimine-containing synthetic models exist at present. An olefin-substituted model (HBMPDI) with an isoelectronic π system has been synthesized.[41] Gas-phase absorption data for this model have been published, as well as solution phase absorption, emission, and on- and off- resonance Raman data.[44] The absorption maximum of gas-phase HBMPDI is at 549 nm. This is close to the absorption maximum of the DsRed protein, which is on the blue end of the range of absorptions recorded for native RFPs.[4] The absorption wavelengths which we have calculated for $\mathbf{R_0}$ are 527 nm for the *trans* conformer and 563 nm for the *cis* conformer. These values are close to the gas-phase absorption of HBMPDI and the blue end of the native RFP absorption range. This suggests to us that our methodology is reasonable. It also suggests that the red-shifted absorption of RFP chromophores relative to GFP chromophores is principally due to the expansion of the π system and not to other properties that acylimines do not share with olefins (such as group electronegativity). The absorption of HBMPDI is blue-shifted in aqueous solution (λ_{max} 482 nm).[48] A similar solvatochromic shift has been reported for GFP chromophore models.[64] CASSCF, CASPT2, and CIS results[39] for the GFP chromophore model HBDI suggest that the shift is related to a stabilization of I^--like resonance structures in a polarizable environment. This is accompanied by stabilization of TICT states in regions of high imidazolinone-bridge bond torsion. This effect is in opposition to those we predict will arise from an acylimine substitution.

HBMPDI possesses weak but detectable fluorescence in aqueous solution (λ_{max} = 565 nm, ϕ = 0.0008).[41] This is interesting because synthetic models of the GFP chromophore do not exhibit steady-state fluorescence in similar conditions.[65] If this result can be extrapolated to the true RFP chromophore structure, then this would be evidence of a higher intrinsic propensity for fluorescence in the RFP chromophore than the GFP chromophore. We believe that such extrapolation is premature. Olefins are less electronegative than acylimines in their ground state. If this holds also for the excited state, then the substituent effects we predict for the acylimine may be weakened or even reversed. In combination with the effects which have been predicted for HBDI in a polarizable environment,[39] it is possible that the active isomerization channels will be qualitatively changed. In the case of HBMPDI, differences

(64) Nielsen, S. B.; Lapierre, A.; Andersen, J. U.; Pedersen, U. V.; Tomita, S.; Anderson, L. H. *Phys. Rev. Lett.* **2001**, *87*, 228102/1.
(65) Chattoraj, M.; King, B. A.; Bublitz, G. U.; Boxer, S. G. *Proc. Natl. Acad. Sci. U.S.A.* **1996**, *93*, 8362.

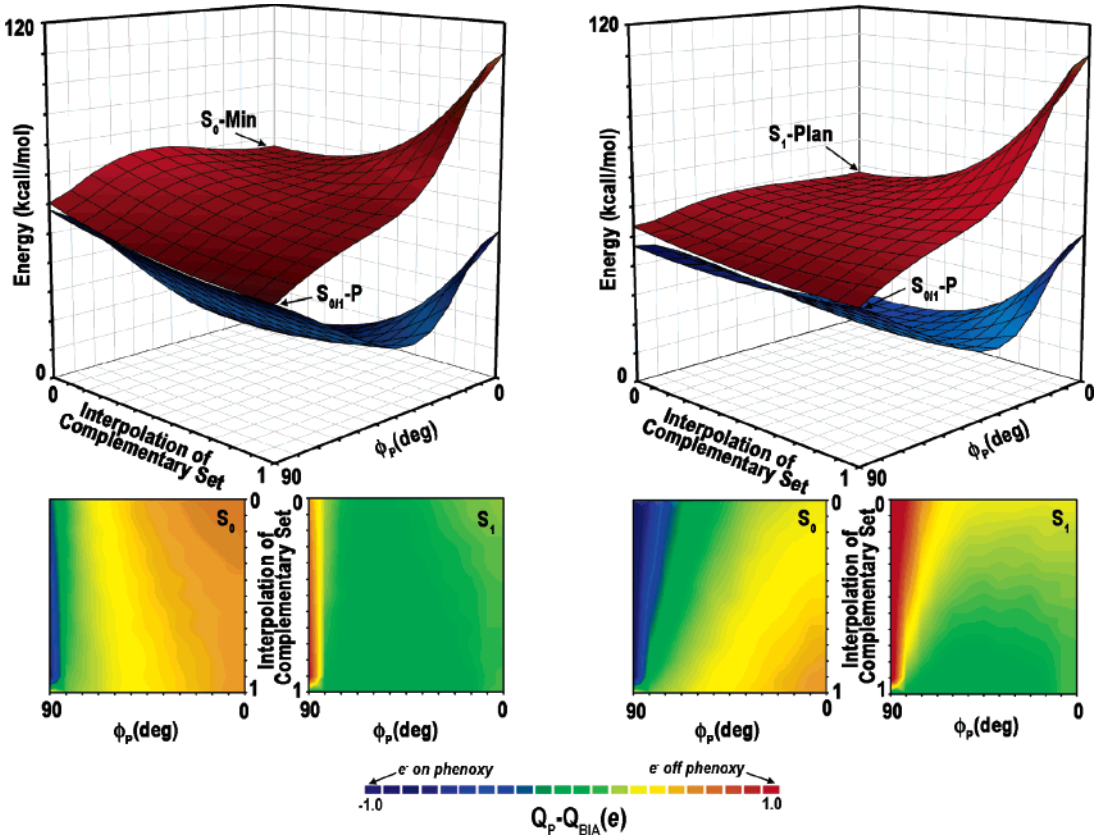

Figure 9. Top: S_0 (blue) and S_1 (red) energies over slices of the potential surfaces of $\mathbf{R_0}$. Surfaces were generated via a bilinear interpolation in internal coordinates. One axis represents the phenoxy-twist dihedral angle ϕ_P, while the other represents simultaneous interpolation of all complementary coordinates. The endpoints defining the interpolation are S_0 minimum (left) and planar S_1 (right) minimum of a *trans* isomer of $\mathbf{R_0}$ and the phenoxy-twisted S_0/S_1 MECI (both plots) of that isomer. Bottom: Differences of Mulliken charges summed on the phenoxy (Q_P) and bridge/imidazolinone/acylimine (Q_{BIA}) sides of the phenoxy-bridge bond in the S_0 (far left, center right) and S_1 (center left, far right) states, plotted over the surface slices above them. Mulliken charge differences are color-coded: negative charge values (electron localization on the phenoxy) are blue, and positive charge differences (localization off the phenoxy) are red.

in the photoisomerization channel could lead to quite different dynamics because of the bulky olefinic substituent on the imidazolinone.

Extrapolation of our results to the protein environment is problematic. Even so, certain results seem to echo patterns which are observed in the RFPs, and these echoes deserve some comment. The first is that nonfluorescent or weakly fluorescent RFPs possess *trans* noncoplanar chromophores.[15,22] Our data are broadly consistent with this pattern, as we predict that the acylimine substituent should stabilize TICT states which lead to photoisomerization of the phenoxy-bridge bond. A pretwisted phenoxy-bridge bond should favor this process by facilitating access to these states.[66] It is interesting that we observe an earlier convergence of the path **P** with a conical intersection seam in the *trans* conformer. If this situation remains in the protein, then the additional torsion needed to reach the intersection seam in proteins with nonplanar chromophores would be slight. Other fluorescent proteins belonging to different subfamilies are known to show a similar connection between chromophore nonplanarity and nonfluorescence; the proteins KFP, asFP595, and amFP486 all display this pattern to some degree.[25,26]

In proteins with a high fluorescence quantum yield, access to internal conversion channels must be denied. If one assumes that similar bridge isomerization channels occur for the chromophore in the protein, then this equates to denial of access to the conical intersection seams which occur in the TICT manifold. One way this could be accomplished is via steric hindrance to rotation. Studies which have addressed steric restrictions in the protein environment for GFP variants indicate that isomerization of the phenoxy-bridge bond or via a proposed hula-twist[67] isomerization may be accommodated by the protein, while isomerization of the imidazolinone-bridge bond may not. Isomerization via hula-twist has been proposed as a volume-conserving pathway for GFP[68] and asFP595[67] chromophores. *Ab initio* potential energy surfaces for the S_1 state of anionic GFP chromophore models do not suggest a stable hula-twist reaction coordinate.[34,38,39] Such motion may arise *in vacuo*, however, due to kinematic effects.[35] We predict that the natural tendency of the RFP chromophore structure is isomerization of the phenoxy-bridge bond, indicating that nonsteric interactions may be responsible for the maintenance of fluorescence in the protein. This could be accomplished, for example, by electrostatic denial of access to the TICT states themselves. It is not clear to us which interactions would accomplish this. Indeed, a feature of all functional fluorescent proteins is a conserved arginine residue which coordinates the imidazolinone oxygen. This interaction would be expected *a priori* to stabilize the TICT states which lead to phenoxy-bridge conversion, since these

(66) Weingart, O.; Buss, V. *Phase Transitions* **2002**, *75*, 19.
(67) Andresen, M.; Wahl, M. C.; Stiel, A. C.; Grater, F.; Schafer, L. V.; Trowitzsch, S.; Weber, G.; Eggeling, C.; Grubmuller, H.; Hell, S. W.; Jakobs, S. *Proc. Natl. Acad. Sci. U.S.A.* **2005**, *102*, 13070.
(68) Maddalo, S. L.; Zimmer, M. *Photochem. Photobiol.* **2006**, *82*, 367.

states would localize the electronic charge closer to the conserved (presumably ionized) arginine. The energy lowering on S_1 en route to the relevant intersections *in vacuo* is within the range of stabilization expected from elementary interactions governing protein structure.[69] Detailed analyses of how RFPs maintain fluorescence will have to come from studies which can treat the protein environment.

The second pattern which deserves consideration is existence of photoconversions in the RFP subfamily which are thought to arise from imidazolinone-bridge bond photoisomerization. Such photoconversions are reported to occur in DsRed[43] and in EqFP611.[42] The initiation of these photoconversions requires illumination at higher intensity or at higher wavelength than that required to provoke simple photoluminescence.[70] This could imply an activated process on the S_1 state or the involvement of a higher excited state. Our goal in this work has been to investigate the effects of the acylimine substitution on the S_1 pathways which are known to exist in GFP chromophore models. Investigation of pathways on higher states is beyond the present scope. Our results indicate a destabilization of the TICT states which lead to imidazolinone-bridge isomerization on S_1. If access to these states is a prerequisite for bond isomerization then our data are consistent with an activated isomerization process on S_1. We have not observed S_0/S_1 intersections associated with a twisted imidazolinone-bridge bond which do not involve the destabilized TICT state. The minimum assumption required to extend our results to photoconversions in the protein is that the isomerization remains activated. Our best estimation of the barrier is within the range of stabilization energies of elementary interactions which govern structure in proteins,[69] so that this assumption should be tested by more calculations which include the protein.

The elucidation of mechanisms by which the protein alters intrinsic chromophore behavior will require methods that can reliably treat a range of protein−chromophore and protein−protein interactions. Many of these interactions will be effectively state-dependent. One possible route is via the application of QM/MM hybrid schemes,[71] which can embed an electronic structure calculation within a classical molecular dynamics force field. Calculations of this type have already been reported for GFP.[37,72] A CASSCF/CASPT2 QM/MM study predicted the absorption and emission of the "I" and "B" states of GFP[65] to an accuracy between 0.21 eV and 0.01 eV depending on the state. The results suggested that the protein stabilizes a gas-phase-like electronic structure by controlling counterion effects. QM/MM techniques coupled with reparametrized semiempirical CAS-CI have also been used to model the photoisomerization of the chromophore within GFP.[37] These studies predicted the induction of a barrier along the pathway, consistent with fluorescence in the protein. These results are encouraging, particularly because they did not attempt to explicitly address the effective state dependence of certain interactions across the QM/MM partition.[73] QM/MM studies of asFP595 have recently appeared.[74,75] These offer a somewhat improved treatment of the cross-boundary electrostatics and Pauli exclusion forces. There are clearly several interactions which future QM/MM developments need to address, including (but are not limited to) proper treatment of fast environmental polarization and charge transfer across the QM/MM boundary. We expect that these interactions may become important for a realistic treatment of RFPs, as suggested by the multiple contributing resonance structures in the Frank−Condon region and the TICT states which mediate internal conversion.

The conformation of the acylimine in our model and in native chromophores deserves some comment. We have found that highly truncated models such as $\mathbf{R_0}$ possess a planar acylimine in their ground and excited states. This is not the case, however, for other models which have appeared in the literature.[3,15] We have found that methylated RFP models such as the one we (and others) have previously used adopt a nonplanar conformation in their ground states. This effect appears to be due to steric interactions between the acylimine oxygen and the methyl substituents. We have found that such models frequently adopt a planar acylimine conformation in their excited state if changes in the geometry of the acylimine relieve the steric constraints.[76] Native chromophores in the RFP subfamily do not possess planar acylimines.[13,15] A detailed analysis of the effect of nonplanar acylimine conformations on the photochemistry is beyond the scope of this paper.

There has been debate in the literature over the significance of the *cis* or *trans* conformation of the acylimine CNCO dihedral angle.[77] Specifically, it has been suggested that inversion of the immature peptide bond may be a prerequisite to maturation of the chromophore in DsRed.[19] This may explain the slow and incomplete chromophore maturation of this protein.[3] Other members of the subfamily, which also possess a *cis* acylimine bond, are reported to completely mature at a much faster rate than DsRed.[78] We have recently reported that the barrier to inversion of the bond is dramatically reduced in the mature acylimine, which suggests that inversion may occur more easily after maturation.[76] Our results indicate that there is little difference to the predicted photoisomerization behavior if the acylimine adopts a *cis* or *trans* conformation (see Supporting Information).

Conclusions

We have reported the first theoretical studies of the bridge photoisomerization of a red fluorescent protein chromophore model. Our results indicate that the electronegative *N*-acylimine substituent which defines the RFP chromophore invokes profound changes on the excited-state pathways which have been previously identified for green fluorescent protein chromophore (GFP) models. Photoisomerization of the imidazolinone-bridge bond is suppressed by the induction of a high barrier on the S_1 surface. Photoisomerization of the phenoxy-bridge bond is favored via stabilization of the S_1 pathway and the convergence of the pathway with an S_0/S_1 conical intersection seam at

(69) Creighton, T. E. *PROTEINS: Structures and Molecular Properties*, 2nd ed.; W. H. Freeman and Co.: New York, 1993.
(70) Cotlet, M.; Hofkens, J.; Habuchi, S.; Dirix, G.; Guyse, M. V.; Michiels, J.; Vanderlyden, J.; Schryver, F. C. D. *Proc. Natl. Acad. Sci. U.S.A.* **2001**, *98*, 14398.
(71) Warshel, A.; Levitt, M. *J. Mol. Biol.* **1976**, *103*, 227.
(72) Sinicropi, A.; Andruniow, T.; Ferré, N.; Basosi, R.; Olivucci, M. *J. Am. Chem. Soc.* **2005**, *127*, 11534.
(73) Ben-Nun, M.; Martinez, T. J. *Chem. Phys. Lett.* **1998**, *290*, 289.
(74) Grigorenko, B.; Savitsky, A.; Topol, I.; Burt, S.; Nemukhin, A. *Chem. Phys. Lett.* **2006**, *424*, 184.
(75) Grigorenko, B.; Savitsky, A.; Topol, I.; Burt, S.; Nemukhin, A. *J. Phys. Chem. B* **2006**, *110*, 18635.
(76) Olsen, S.; Smith, S. C. *Chem. Phys. Lett.* **2006**, *426*, 159.
(77) Zaveer, M. S.; Zimmer, M. *Bioorg. Med. Chem. Lett.* **2003**, *13*, 3919.
(78) Wiedenmann, J.; Schenk, A.; Röcker, C.; Glrod, A.; Spindler, K.-D.; Nienhaus, G. U. *Proc. Natl. Acad. Sci. U.S.A.* **2002**, *99*, 11646.
(79) Humphrey, W.; Dalke, A.; Schulten, K. *J. Mol. Graphics* **1996**, *14*, 33.

intermediate values of the bond torsion. These effects are due to the action of the strongly electronegative acylimine on the twisted intermolecular charge-transfer (TICT) states which are encountered along the pathways. Our results are further evidence of the importance of TICT states and charge-transfer intersections in the control of photoisomerization processes in fluorescent protein chromophores.

Acknowledgment. We wish to thank Dr. Mark Prescott for extensive and illuminating discussions of various aspects of RFP biochemistry. The calculations described in this work were carried out at the CCMS/Hypersonics Supercomputing Facility at the University of Queensland and at the Australian Partnership for Advanced Computing (APAC) National Facility in Canberra. Time on the APAC machines was generously granted through the Merit Allocation Scheme and through a Queensland Cyber Infrastructure Foundation (QCIF) partner-share grant. This work has been partially supported by funds granted through the ARC/NHMRC Research Network "Fluorescence Applications in Biotechnology and Life Sciences" (RN0460002). Some of the graphics used in the figures here were generated using VMD.[79]

Supporting Information Available: Complete ref 54, Cartesian coordinates, absolute S_0 and S_1 energies, graphical representations of active space orbitals and orbital occupation numbers for all potential surface extrema and conical intersection structures described in the text, and internal coordinate representations used for interpolation surfaces. This material is available free of charge via the Internet at http://pubs.acs.org.

JA066430S